

See discussions, stats, and author profiles for this publication at: <https://www.researchgate.net/publication/7672883>

Two-Dimensional Measurement of Proton T₁ ρ Relaxation in Unlabeled Proteins: Mobility Changes in α-Bungarotoxin upon Binding of an Acetylcholine Receptor Peptide †

ARTICLE *in* BIOCHEMISTRY · SEPTEMBER 2005

Impact Factor: 3.02 · DOI: 10.1021/bi050645h · Source: PubMed

CITATIONS

5

READS

65

3 AUTHORS, INCLUDING:



Abraham O Samson

Bar Ilan University

19 PUBLICATIONS 307 CITATIONS

SEE PROFILE



Jordan H Chill

Bar Ilan University

38 PUBLICATIONS 597 CITATIONS

SEE PROFILE

Two-Dimensional Measurement of Proton $T_{1\rho}$ Relaxation in Unlabeled Proteins: Mobility Changes in α -Bungarotoxin upon Binding of an Acetylcholine Receptor Peptide[†]

Abraham O. Samson, Jordan H. Chill,[‡] and Jacob Anglister*

Department of Structural Biology, Weizmann Institute of Science, Rehovot 76100, Israel

Received April 7, 2005; Revised Manuscript Received June 23, 2005

ABSTRACT: A method for the measurement of proton $T_{1\rho}$ relaxation times in unlabeled proteins is described using a variable spin-lock pulse after the initial nonselective 90° excitation in a HOHAHA pulse sequence. The experiment is applied to α -bungarotoxin (α -BTX) and its complex with a 25-residue peptide derived from the acetylcholine receptor (AChR) α -subunit. A good correlation between high $T_{1\rho}$ values and increased local motion is revealed. In the free form, toxin residues associated with receptor binding according to the NMR structure of the α -BTX complex with an AChR peptide and the model for α -BTX with the AChR [Samson, A. O., et al. (2002) *Neuron* 35, 319–332] display high mobility. When the AChR peptide binds, a decrease in the relaxation times and the level of motion of residues involved in binding of the receptor α -subunit is exhibited, while residues implicated in binding γ - and δ -subunits retain their mobility. In addition, the quantitative $T_{1\rho}$ measurements enable us to corroborate the mapping of boundaries of the AChR determinant strongly interacting with the toxin [Samson, A. O., et al. (2001) *Biochemistry* 40, 5464–5473] and can similarly be applied to other protein complexes in which peptides represent one of the two interacting proteins. The presented method is advantageous because of its simplicity, generality, and time efficiency and paves the way for future investigation of proton relaxation rates in small unlabeled proteins.

NMR¹ relaxation times are influenced by the global tumbling of the molecules as well as by local motions. Such relaxation times include the longitudinal relaxation time (T_1), commonly called the laboratory frame spin–lattice relaxation time, the transverse relaxation time (T_2), also known as spin–spin relaxation, and the spin–lattice relaxation time in the rotating frame ($T_{1\rho}$) characterized by the decay of magnetization spin-locked by a radio frequency field ($\omega_1 = \gamma B_1$) applied in a manner that is perpendicular to B_0 . Relaxation of the transverse magnetization in the laboratory frame (T_2) and the longitudinal magnetization in the rotating frame ($T_{1\rho}$) also depend on conformational and chemical exchange.

The efficiency of the relaxation by dipole–dipole interactions, chemical shift anisotropy, and scalar interactions, all

of which are major contributors to relaxation, depends on the correlation times of the nuclei that are involved. Protein residues involved in secondary structure usually exhibit T_2 and $T_{1\rho}$ values that are determined mostly by the overall tumbling rate of the molecule. Flexible regions and the unstructured segment of the protein exhibit T_2 and $T_{1\rho}$ values that are typically higher than those exhibited by rigid segments (1–3). Ligand binding is often accompanied by altered flexibility of the domains involved in binding, changes that effect local flexibility and therefore can be probed by T_2 or $T_{1\rho}$ measurements. Thus, measurements of T_1 , T_2 , $T_{1\rho}$, and NOE can provide insight into the dynamics of proteins in solution and changes occurring upon ligand binding.

Studies of dynamic processes by NMR have traditionally focused on measurements of the relaxation parameters of ^{15}N and ^{13}C nuclei bonded to ^1H using isotope-labeled proteins. Proton relaxation times in unlabeled proteins have not been investigated as thoroughly. This can be attributed to several factors, including the difficulty in measurements and data analysis due to spectral overlap. It is also difficult to interpret the T_2 and $T_{1\rho}$ data and analyze the type and time scale of motions contributing to relaxation because each proton may relax through several different pathways such as scalar couplings and dipole–dipole interactions with multiple nearby protons (4). Nevertheless, several laboratories measured proton relaxation in proteins. Bodenhausen and co-workers (5–7) described several different experiments for measurements of longitudinal and transverse relaxation

[†] This study was supported by NIH Grant NS38301. J.A. is the Dr. Joseph and Ruth Owades Professor of Chemistry.

* To whom correspondence should be addressed. Telephone: +972-8-9343394. Fax: +972-8-9344136. E-mail: jacob.anglister@weizmann.ac.il.

[‡] Present address: Laboratory of Chemical Physics, National Institute of Diabetes and Digestive and Kidney Diseases, National Institutes of Health, Bethesda, MD 20892.

¹ Abbreviations: 1D, one-dimensional; 2D, two-dimensional; α -BTX, α -bungarotoxin; ACh, acetylcholine; AChR, acetylcholine receptor; COSY, correlation spectroscopy; CPMG, Carr–Purcell–Meiboom–Gill experiment; HOHAHA, homonuclear Hartman–Hahn spectroscopy; IR, inverse recovery; NMR, nuclear magnetic resonance; NOESY, nuclear Overhauser enhancement spectroscopy; ROESY, rotating frame Overhauser spectroscopy; SL, spin-lock; T_1 , spin–lattice, longitudinal relaxation time in the laboratory frame; $T_{1\rho}$, spin–lattice, longitudinal relaxation time in the rotating frame; T_2 , spin–spin, transverse relaxation time; TOCSY, total correlation spectroscopy.

times of selected protons. These experiments enabled accurate determination of relaxation times of specific protons. However, it was impractical to apply these 1D experiments for measurements of a large number of protons. Arseniev and co-workers successfully measured T_1 relaxation times for most of the protons of a small 15-residue peptide gramicidin using a series of inverse-recovery (IR) 2D COSY experiments (8). In this method, H^N , H^α , H^β , and methyl protons were classified into groups with distinctive longitudinal relaxation times. Instead of using a series of 2D measurements with variable intervals during which the magnetization recovers to thermal equilibrium due to longitudinal relaxation, Kay and Prestegard suggested the use of a single 2D "accordion" experiment (9). In this experiment, T_1 values were extracted from the line shapes of cross-peaks as described in detail by Bodenhausen and Ernst (10, 11). Using such a T_1 -accordion COSY experiment, the location of divalent ion binding sites in the acyl-carrier protein was determined on the basis of relaxation time enhancements following paramagnetic ion replacement (12). In this method, however, not all proton relaxation times were assigned quantitatively. Employing 1D-inverse-recovery experiments, longitudinal relaxation times of amide protons were also measured in a protein that was highly deuterated to prevent relaxation through spin diffusion (13). A method for monitoring DNA rigidity by determining the $T_{1\rho}$ relaxation times of nucleotide protons was described by Wang et al. (14). Several 1D experiments consisting of a 90° pulse followed by a variable-length SL were acquired to determine the relaxation values. Schmitz et al. (15) and Kennedy et al. (16) also utilized the rotating frame spin-lattice relaxation to address DNA mobility. T_1 and T_2 relaxation rates were measured using conventional 1D IR techniques and CPMG experiments. Proton $T_{1\rho}$ relaxation has been utilized to determine internal mobility in glycylglycine (17), enkephalin (18), and cyclic peptides (19, 20). Recently, Schleucher and Wilmenga suggested the use of off-resonance ROESY experiments in detecting internal motion in unlabeled proteins on the 100 ps time scale (21). A series of off-resonance ROESY experiments were applied on BPTI and revealed internal motions of 75 individual long- and short-range H-H vectors. Torchia and co-workers used amide proton $T_{1\rho}$ measurements in uniformly ^{15}N -labeled HIV-1 protease to study millisecond time scale motions (4). To reduce the extent of cross-relaxation and obtain a relatively larger contribution to relaxation from exchange, the protease was uniformly deuterated, thus suppressing most of the cross-relaxation pathways (4). While the multitude of methodologies presented in the aforementioned studies underlines the importance of proton $T_{1\rho}$ measurement, the 1D methods that were used for unlabeled proteins are hopelessly incapable of assessing larger proteins. These studies therefore advocate the need for a simple and general 2D technique by which the $T_{1\rho}$ of all residues in a relatively large macromolecule (<12 kDa) could be determined without requiring isotope labeling.

The nicotinic acetylcholine receptor (AChR) is a ligand-gated cation channel that is activated upon binding of the neurotransmitter acetylcholine (ACh). It is a 290 kDa membrane glycoprotein consisting of five homologous subunits, $\alpha\delta\beta\alpha\gamma$ (22, 23), with two ACh binding sites formed at the α - δ and α - γ subunit interfaces (24). The α -subunit

of the muscle AChR ($\alpha 1$) also contains a high-affinity binding site for antagonists such as α -bungarotoxin (α -BTX) (25). α -BTX is a 74-amino acid, 8 kDa α -neurotoxin derived from the snake venom of *Bungarus multicinctus*. It binds strongly to the postsynaptic muscle AChR with an IC_{50} value of 3.5×10^{-10} M (26), competitively inhibiting ACh binding and thereby blocking neuromuscular transmission. Synthetic peptide analogues corresponding to a linear segment of the α -subunit form tight complexes with α -BTX (26–32). The structure of an AChR peptide in complex with α -BTX, a complex containing a total of 99 amino acid residues, was determined using homonuclear 2D NMR (33). The overall structure of the toxin consists of a three-finger motif with a C-terminal tail. The AChR peptide folds into a β -hairpin which associates with the triple-stranded antiparallel β -sheet core of the toxin to form a five-stranded intermolecular β -sheet. The formation of intermolecular hydrogen bonds together with multiple hydrophobic interactions and cation- π interactions account for the high affinity of the toxin for the AChR peptides. The off-rate of a peptide comprising residues $^{\alpha}\text{W184}$ – $^{\alpha}\text{D200}$ of the AChR was found to be $1.1 \times 10^{-4} \text{ s}^{-1}$ (34) [α -BTX and AChR residues are designated by a superscript B and α (i.e., $^{\text{B}}\text{X}$ or $^{\alpha}\text{X}$), respectively, before the amino acid type and position in sequence].

In the past, we have employed differences in $T_{1\rho}$ relaxation times in studying protein complexes with peptides. A $T_{1\rho}$ -filtered NOESY experiment was used to obtain a transferred-NOE spectrum of a peptide bound to an antibody (35). A 30 ms SL pulse applied after the first 90° pulse eliminated all the cross-peaks due to intramolecular interactions within the 50 kDa antibody Fab fragment, and only transferred NOE cross-peaks due to antibody-peptide interactions and interactions within the bound peptide were observed (35). In another type of experiment, a combination of HOHAHA and ROESY spectra with long mixing period was used to map the epitope of a gp120 V3-loop peptide interacting with an HIV-1 neutralizing antibody (36). Similarly, we mapped the exact segment of an AChR peptide interacting with α -BTX to the $^{\alpha}\text{W184}$ – $^{\alpha}\text{D200}$ segment using NMR dynamic filtering techniques (32). HOHAHA and ROESY spectra of the α -BTX–AChR peptide complex acquired with long mixing times highlighted the peptide residues that did not interact with the toxin and retained considerable mobility upon binding to α -BTX. In these two approaches, the duration of the spin-lock pulses and the mixing period in the HOHAHA and ROESY experiments were adjusted to obtain optimal discrimination between the protein and the peptide cross-peaks. However, there was no attempt to quantitatively characterize the $T_{1\rho}$ relaxation times of the interacting molecules.

Here we present a simple homonuclear 2D method for measuring proton $T_{1\rho}$ relaxation times based on the HOHAHA experiment (37). Using this method, we characterized for the first time changes in relaxation times of a snake neurotoxin upon binding of an AChR peptide. A decrease in the relaxation times and the mobility of residues involved in binding of the receptor α -subunit are exhibited, while residues implicated in binding the γ - and δ -subunits retain their mobility (33). In addition, the quantitative $T_{1\rho}$ measurements enable us to corroborate the mapping of boundaries of the AChR determinant strongly interacting with the toxin.

EXPERIMENTAL PROCEDURES

NMR Sample Preparation. α -BTX was purchased from Sigma and did not require further purification. The toxin was dissolved in a 90% H₂O/10% D₂O mixture and 0.05% NaN₃ and acidified with HCl to pH 4. The final concentration of the α -BTX in the NMR sample was 0.5 mM. The AChR peptide, EERGWKHWVYYTCCPDTPYLDITEE, corresponding to residues 182–202 of the $\alpha 1$ subunit of the *Torpedo californica* AChR and elongated with two glutamic acid residues at each terminus to increase solubility, was synthesized and purified as previously described (32). The toxin–peptide complex was prepared and purified as described previously (32). The purified and lyophilized complex was dissolved in a 90% H₂O/10% D₂O mixture and 0.05% NaN₃ and acidified with HCl to pH 4. The final concentration of the complex in the NMR sample was 2 mM.

NMR Spectroscopy. NMR spectra of α -BTX and its complex were acquired on a Bruker DRX 800 MHz spectrometer at 30 °C. Measurements of the AChR peptide were carried out on a 500 MHz spectrometer. The experiment used for the 2D $T_{1\rho}$ measurements was based on the HOHAHA pulse sequence (37, 38) and incorporated a SL pulse after the initial 90° pulse. The $T_{1\rho}$ -filtered HOHAHA spectra were measured utilizing the following pulse sequence: 90_x–SL_y–evolution (t_1)–(WALTZ)–acquisition (t_2). Measurements of free α -BTX and its complex with the AChR peptide were performed on an 800 MHz spectrometer. Isotropic mixing was realized using a WALTZ (39) pulse sequence with a short duration of 30 ms. The spectra were acquired using sensitivity enhancement and TPPI, and the water signal was suppressed by the WATERGATE pulse sequence (water suppression by gradient-tailored excitation) (40).

A series of six experiments was measured with SL durations varying from 0 to 25 ms in 5 ms increments. The number of complex points acquired on the 500 MHz spectrometer were 2048 and 256 in the F_2 and F_1 dimensions, respectively, with spectral widths of 6000 Hz. The numbers of complex points acquired on the 800 MHz spectrometer were 8192 and 800 in the F_2 and F_1 dimensions, respectively, with spectral widths of 11,160 Hz. All spectra were processed and analyzed using NMRDraw and NMRPipe (41). Unresolved peaks at frequencies close to that of the water required additional baseline correction using polynomial water subtraction in all experiments. Linear prediction in the F_1 dimension was also performed to increase resolution and improve the automated peak picking. Automated peak picking in these spectra was achieved using NMRPipe and in-house Perl scripts. Sequential assignment of the toxin and its peptide complex was performed according to common procedures (42) at 30 °C.

Data Analysis. Proton $T_{1\rho}$ values were determined by fitting the relaxation data to a single-exponential decay [$I(t) = I_0 \exp(-t/T_{1\rho})$] using the modelXY package (41). Error values to be included in the calculation were obtained from signal-to-noise ratios. The per residue change in the accessible surface of the peptide in the α -BTX–AChR peptide complex (PDB entry 1L4W) was calculated using the homology module of Insight II (Accelrys). The display of the α -BTX–AChR peptide structure with a radius proportional to the $T_{1\rho}$ value was created using Molmol (43).

RESULTS

Pulse Sequence. The proposed pulse sequence that measures $T_{1\rho}$ values contains a SL pulse after the initial 90° pulse. During this SL pulse, the initial magnetization (M_0) is characterized by an exponential decay:

$$M(t_{\text{SL}}) = M_0 \exp(-t_{\text{SL}}/T_{1\rho})$$

During the mixing period, further relaxation occurs, and the final relaxation is roughly proportional to

$$M(t_{\text{SL}}, \tau_m) = M_0 \exp(-t_{\text{SL}}/T_{1\rho}) \exp(-\tau_m/T_{1\rho})$$

The mixing time (τ_m) in the set of experiments is constant, and as a result, the cross-peak intensity decays exponentially according to $T_{1\rho}$ with an increase in t_{SL} .

The proposed experiment, in which the spin-lock pulse is applied before the evolution period, is an extension to two dimensions of the conventional 1D experiment used to measure nonselective $T_{1\rho}$. The 2D experiment has the advantage in that it spreads the spectrum of the protein into two dimensions and allows measurements of $T_{1\rho}$ values of individual protons in small unlabeled proteins. Other than the increased resolution, the proposed 2D method has the same advantages and drawbacks as the 1D experiment commonly used for nonselective $T_{1\rho}$ measurements.

For long SL pulses, proton magnetization may not be characterized by a single-exponential decay because of scalar interactions and spin diffusion. Indeed, deviations from single-exponential decay were observed utilizing SL pulses of 100 and 200 ms. However, the initial relaxation rates measured using short SL pulses are good approximations of the true self-relaxation rates (44, 45) and are better characterized by a single-exponential decay (44, 45). Therefore, short spin-lock pulses of up to 25 ms were used herein to obtain $T_{1\rho}$ relaxation times. In addition, a short isotropic mixing time of 25 ms was utilized to minimize signal decay due to magnetization transfer to protons more than three bonds apart. As a result, the $T_{1\rho}$ -filtered HOHAHA spectrum displayed strong H^N–H ^{α} cross-peaks and few long-range correlations. A section of the HOHAHA spectrum of free α -BTX used for the $T_{1\rho}$ determination is displayed in Figure 1.

The decay of the intensity of the H ^{α} (F_1)–H^N(F_2) cross-peaks which are above the diagonal is governed by the relaxation rate of H ^{α} protons, and the intensity of the H^N(F_1)–H ^{α} (F_2) cross-peaks which are below the diagonal is governed by the relaxation rate of H^N protons. (F_2 represents the acquisition dimension.) Since most H^N(F_1)–H ^{α} (F_2) cross-peaks are weakened by the water suppression scheme that dephases water magnetization prior to acquisition, thereby reducing the intensity of all resonances up to 1 ppm away from the water, we concentrated on measuring the decay of the symmetrical H ^{α} (F_1)–H^N(F_2) cross-peaks at the frequency governed by the $T_{1\rho}$ relaxation rates of the H ^{α} protons.

Spectral Processing. Well-resolved spectra are a prerequisite for the automated peak picking process. As a measure of precaution, the spectral resolution was further increased through processing using squared sine-bell window functions, zero filling, and linear prediction. Without these measures, automated peak picking is less accurate, leading in several cases to poor fits to the exponential decay. Signal apodization using a squared cosine-bell window function or a squared

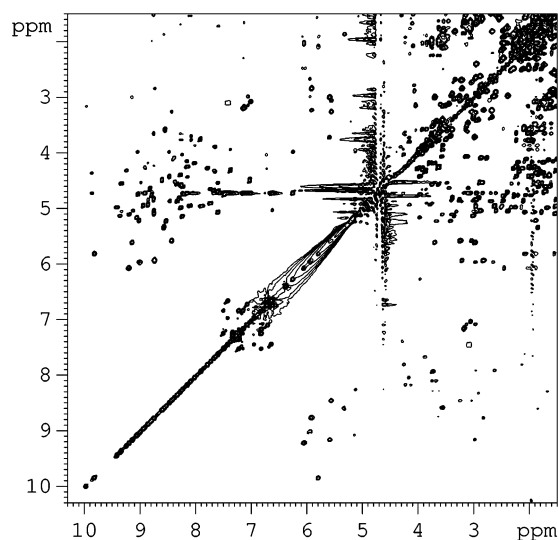


FIGURE 1: $T_{1\rho}$ -filtered HOHAHA spectrum of free α -BTX. The spectrum was measured on an 800 MHz spectrometer at 30 °C with a spin-lock pulse applied after the initial 90° pulse. The duration of the spin-lock pulse was 25 ms. Notice the absence of the majority of the $H^N(F_2)$ – $H^N(F_1)$ cross-peaks due to the water suppression scheme.

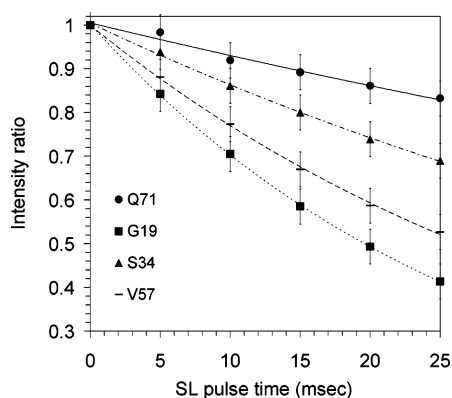


FIGURE 2: Single-exponential fit to the proton $T_{1\rho}$ relaxation data. The single-exponential fit to the decay of cross-peak intensity for residues BQ71 , BG19 , BS34 , and BV57 of unbound α -BTX is plotted as a function of the spin-lock duration. The spectra used for this analysis were recorded at 30 °C on an 800 MHz spectrometer. Errors were estimated from signal-to-noise ratios in the spectra. Fitted exponential curves are shown.

cosine shifted by 45° did not result in any significant changes in the determined $T_{1\rho}$ values.

$T_{1\rho}$ Measurements. To calculate the $T_{1\rho}$ values, the decay in cross-peak intensity as a function of the SL pulse was fitted to a monoexponential curve with minor deviations (Figure 2). The error in peak intensity was estimated to be approximately 4% based upon the noise in empty areas of the spectra. Most cross-peaks displayed very good fits to the exponential curve, and the estimated error in $T_{1\rho}$ determination was 11% on average. Cross-peaks of the geminal protons of glycine residues typically gave rise to two similar $T_{1\rho}$ values. The $T_{1\rho}$ values of a few residues that did not give rise to cross-peaks in the spectra (i.e., proline residues and BI1 and E180 , the N-terminal residues of the toxin and peptide, respectively) or that were poorly resolved could not be determined. Poorly resolved residues include BT8 , BT62 , and BD63 in the complex as well as BS9 , BD30 , and BA31 in the unbound state.

For the vast majority of the protons, a single-exponential decay could be easily fitted to the relaxation curve. Deviation from single-exponential decay could occur in principle despite the short spin-lock pulse if spin diffusion occurs. We assessed the contribution of this possible effect to $T_{1\rho}$ relaxation by repeating our experiment with the spin-lock and evolution blocks reversed (4) as follows: 90°–evolution (t_1)–SL_y–(WALTZ)–acquisition (t_2).

Since off-diagonal ROESY peaks appeared in this experiment solely for the nearest protons when a 25 ms spin-lock pulse was applied, we conclude that multispin effects are suppressed in our $T_{1\rho}$ measurements, justifying our assumption of monoexponential behavior for the initial relaxation rates.

Determination of $T_{1\rho}$ Values of H^N Protons of Free α -BTX. The $T_{1\rho}$ values of the H^N protons of free α -BTX obtained on the 800 MHz are summarized in Figure 3A. The average $T_{1\rho}$ values of H^N protons in free α -BTX are 50 and 37 ms for all residues and for β -strand residues, respectively. Two segments of the toxin exhibit unusually long H^N $T_{1\rho}$ relaxation times (≥ 100 ms), namely, BS35 and BR36 located at the tip of the second finger, and BQ71 – BG74 at the C-terminus. Moderately long $T_{1\rho}$ relaxation times (≥ 60 ms) are exhibited by residues at the tip of the first finger, at the tip of the second finger, and at the N-terminal strand of the third finger. These results are in agreement with previous model-free-based dynamics studies of a three-finger toxin that found that the tips of the three fingers as well as the N-terminal segment of the third finger exhibited low order parameters (46, 47).

Determination of $T_{1\rho}$ Values of H^N Protons of α -BTX in Complex with the AChR Peptide. The $T_{1\rho}$ values of the H^N protons of α -BTX in complex with the AChR peptide are summarized in Figure 3B. The average $T_{1\rho}$ values for all residues and β -strand residues are 35 and 28 ms, respectively. The decreases in average $T_{1\rho}$ values in comparison to those obtained for free α -BTX are consistent with the 35% change in molecular weight occurring upon complex formation. Exceptionally large decreases in $T_{1\rho}$ relaxation times are displayed by C-terminal residues BK70 (from 64 to 25 ms), BQ71 (from 129 to 54 ms), BR72 (from 150 to 51 ms), and BG74 (from 148 to 50 ms). The decreased mobility of most of the residues at the C-terminal segment in the α -BTX–AChR peptide complex (Figure 3C) can be explained by the interactions of BH68 , BP69 , BK70 , and BQ71 with the AChR peptide (33). In addition to the C-terminal residues, BR36 and BK38 of the second finger exhibited a dramatic decrease in their $T_{1\rho}$ relaxation time upon binding to the AChR peptide (from 100 to 31 ms for BR36 and from 50 to 18 ms for BK38) (Figure 3). A significant decrease in $T_{1\rho}$ is experienced also by the H^N proton of BC29 (from 50 to 23 ms) which together with BK38 extends the β -hairpin of toxin finger II upon complex formation (48). A significant decrease in $T_{1\rho}$ is observed also for residues of the first toxin finger, BT6 (from 43 to 26 ms), BA7 (from 67 to 37 ms), and BI11 (from 31 to 21 ms), which were found to interact with the AChR peptide. The change in the exposed surface upon complex formation of the toxin presented in Figure 3D is correlated with the change in $T_{1\rho}$ relaxation times (Figure 3C). The 2D $T_{1\rho}$ experiment enabled us to determine the relaxation times of several amide protons using the symmetrical $H^N(F_1)$ – $H^N(F_2)$ peaks when those were sufficiently distant from the

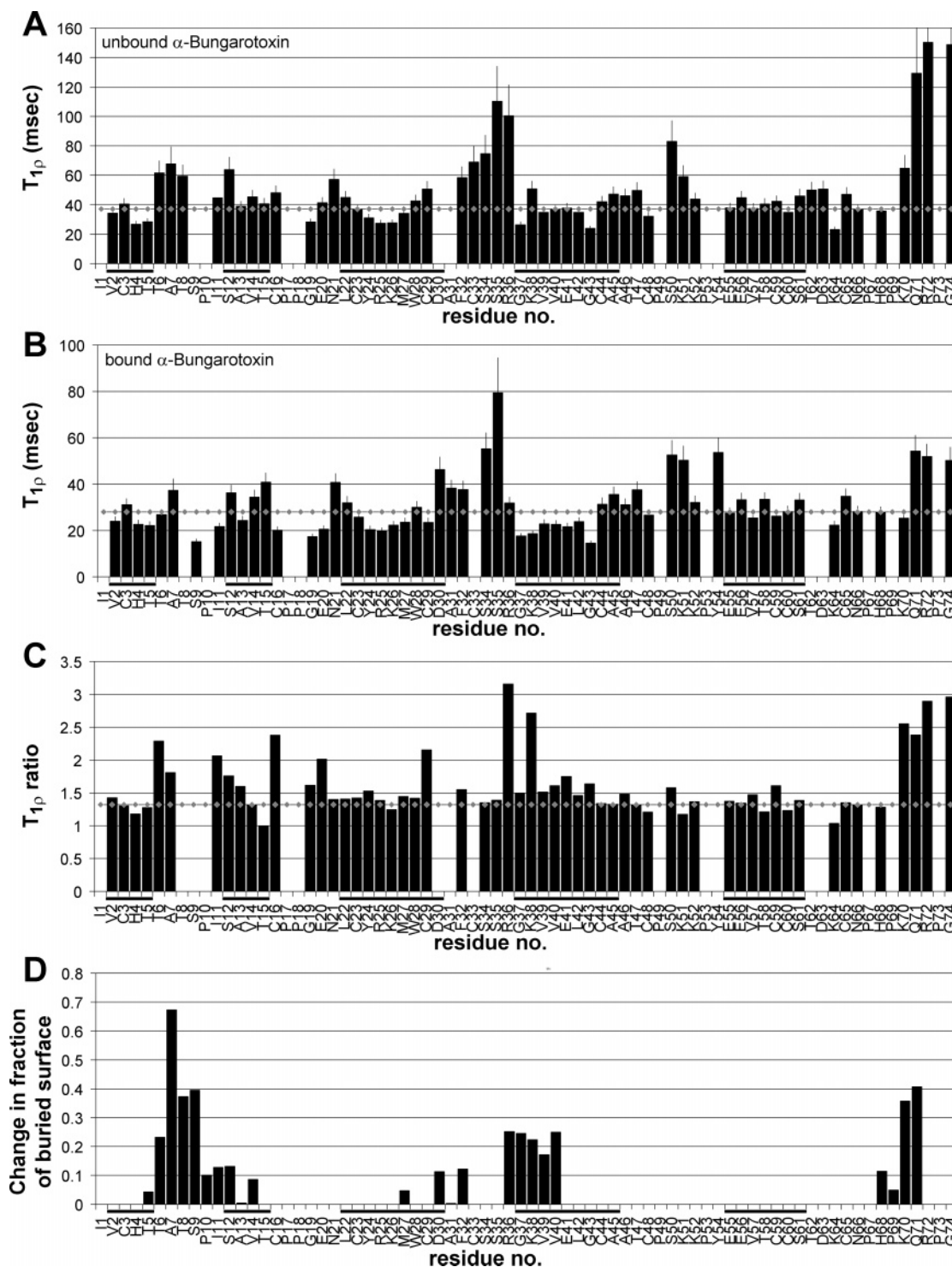


FIGURE 3: Changes in $T_{1\rho}$ values of H^{α} protons in free and bound α -BTX. (A) $T_{1\rho}$ values for each residue in the free toxin. Small diamonds denote the average $T_{1\rho}$ of β -sheet residues (37 ms). (B) $T_{1\rho}$ values for each residue in the bound toxin. Small diamonds denote the average $T_{1\rho}$ of β -sheet residues (28 ms). Errors in $T_{1\rho}$ values are displayed as error bars. (C) Ratio between the $T_{1\rho}$ values for each residue in the free and bound α -BTX. Small diamonds denote the ratio between the average $T_{1\rho}$ values of the β -sheet residues in the free and bound toxin (1.32). All values were measured on the 800 MHz spectrometer at 30 °C. Solid horizontal lines beneath the residue axis indicate β -sheet structure. (D) Fractional decrease in the exposed surface area upon complex formation for each α -BTX residue.

water resonance to be unaffected by solvent suppression. These $T_{1\rho}$ values were similar to those obtained for the H^{α} protons of the corresponding residues.

Determination of $T_{1\rho}$ Values of H^{α} Protons of the Free and α -BTX-Bound AChR Peptide. The $T_{1\rho}$ profile of the AChR peptide in its free form is presented in Figure 4A. The peptide exhibits relatively long relaxation times with an average $T_{1\rho}$ of 155 ms. Most of the peptide residues, excluding the

C-terminal residue, display $T_{1\rho}$ relaxation times of 90–160 ms. The C-terminal segment, $^{\alpha}\text{D200}$ – $^{\alpha}\text{E204}$, exhibits gradually increasing $T_{1\rho}$ values, ranging from 204 ms for $^{\alpha}\text{D200}$ to 352 ms for $^{\alpha}\text{E204}$. The low relaxation rates and therefore long relaxation times at the termini are typical of a small polymer and peptides with unrestrained termini (49, 50).

The $T_{1\rho}$ measurements of the AChR peptide in complex with α -BTX presented in Figure 4B confirm the previous

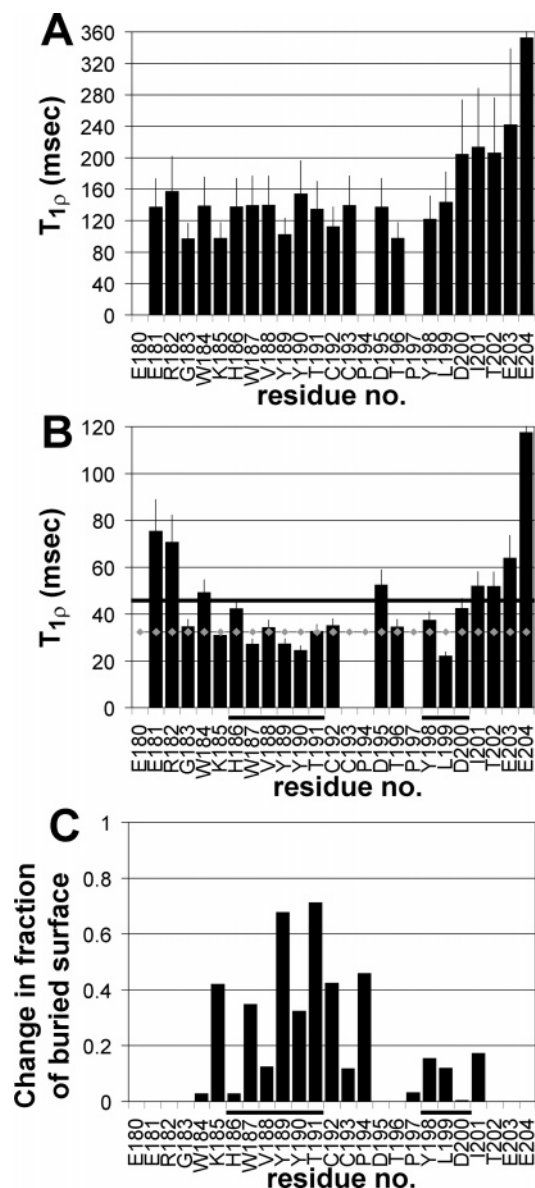


FIGURE 4: Comparison between $T_{1\rho}$ values of H^{α} protons in the free and bound AChR peptide and changes in the exposed surface upon binding. (A) $T_{1\rho}$ values of each residue in the free AChR peptide. (B) $T_{1\rho}$ values for each residue in the AChR peptide in complex with the toxin. The spectra of the free and bound AChR peptide were measured at 30 °C on 500 and 800 MHz spectrometers, respectively. Errors in $T_{1\rho}$ values are displayed as error bars. The average $T_{1\rho}$ value of 32.3 ms for the peptide residues in β -strands is denoted in panel B with small squares, and the 45 ms threshold used to differentiate between the peptide residues interacting with the toxin and those that do not is drawn as a horizontal line. (C) Fractional decrease in the exposed surface for residues in the AChR peptide. Solid lines beneath the residue axis represent β -sheet structure.

mapping of the AChR determinant (32). The $T_{1\rho}$ values of the AChR peptide vary from 115 ms for $^{\alpha}\text{E204}$ to 21.9 and 20.3 ms for $^{\alpha}\text{L199}$ and $^{\alpha}\text{K185}$, respectively. Residues outside the binding determinant (excluding residue $^{\alpha}\text{G183}$ mentioned below), namely, $^{\alpha}\text{E181}$, $^{\alpha}\text{R182}$, $^{\alpha}\text{W184}$, $^{\alpha}\text{I201}$, $^{\alpha}\text{T202}$, $^{\alpha}\text{E203}$, and $^{\alpha}\text{E204}$, exhibit $T_{1\rho}$ values above an arbitrary threshold value of 45 ms. Residues within the binding determinant, $^{\alpha}\text{K185}$ – $^{\alpha}\text{D200}$, with the exception of $^{\alpha}\text{D195}$, display $T_{1\rho}$ values of <45 ms (Figure 4B), similar to the values for most of the toxin protons. These values quantitatively define the residues constituting the binding determinant of the AChR

and account for their absence in the $T_{1\rho}$ -attenuated HOHAHA and ROESY experiments. Interestingly, $^{\alpha}\text{D195}$ exhibits an increased $T_{1\rho}$ of 52 ms that can be correlated with the absence of interactions with the toxin and the inferred flexibility of this residue. $^{\alpha}\text{D195}$ and $^{\alpha}\text{T196}$ were found to form a β -bulge in the complex with the toxin, and no interactions between them and the toxin could be detected, thus explaining the relatively high $T_{1\rho}$ values observed for these two residues close to the center of the AChR determinant interacting with the toxin (33). In general, the change in the exposed surface upon binding of the AChR peptide presented in Figure 4C is correlated with the change in $T_{1\rho}$ times (Figure 4A,B).

$T_{1\rho}$ Values of Glycine Residues. Glycine residues exhibit short $T_{1\rho}$ values which differ considerably from those of their adjacent residues due to the strong dipole–dipole interactions between the geminal H^{α} protons. Nevertheless, glycine $T_{1\rho}$ values display the same correlation with the α -BTX structure. Thus, glycines $^{\text{B}}\text{G19}$, $^{\text{B}}\text{G37}$, and $^{\text{B}}\text{G43}$, located in the structured regions of the complex, exhibit an average $T_{1\rho}$ of 17 ms in the bound state. In contrast, toxin residue $^{\text{B}}\text{G74}$ (50 ms) and peptide residue $^{\alpha}\text{G183}$ (34 ms) located at the termini of the toxin and peptide, respectively, have far longer $T_{1\rho}$ values. We therefore conclude that a comparison between glycine residues at the different positions in the complex can be used to qualitatively evaluate the variation in their dynamics.

A Simplified Spectrum for $T_{1\rho}$ Measurements of Mobile Residues Obtained Using a Long WALTZ Pulse Train. In complexes of large proteins with peptide ligands, the overlap with the protein cross-peaks would hamper quantitative $T_{1\rho}$ measurements of the flexible segments of the peptide that do not interact with the protein. Elimination of the protein cross-peaks as well as cross-peaks of the peptide residues strongly interacting with the protein could be achieved by increasing the duration of the WALTZ pulse trains. To demonstrate the feasibility of $T_{1\rho}$ measurements of flexible domains in large protein and their complexes, we determined the $T_{1\rho}$ relaxation times when the duration of the WALTZ pulse train is 100 and 200 ms and compared the results to those obtained when the duration of the WALTZ is 30 ms. No significant changes in the $T_{1\rho}$ values were observed when a different duration of the WALTZ is used. However, a 200 ms WALTZ eliminated most of the background from α -BTX and highlighted the residues of the peptide that do not interact with the toxin and the mobile regions in the toxin itself (Figure 5). Thus, long WALTZ trains can be used to simplify the spectra and enable more accurate epitope mapping and quantitative determination of $T_{1\rho}$ in flexible domains possibly even for large proteins and their complexes.

Comparison of $T_{1\rho}$ Values Obtained by 1D Methods. To further validate the proposed method, we determined the $T_{1\rho}$ values of five amide protons ($^{\text{B}}\text{K70}$, $^{\text{B}}\text{K64}$, $^{\text{B}}\text{K26}$, $^{\text{B}}\text{C29}$, and $^{\alpha}\text{V188}$) as well as three H^{α} protons ($^{\text{B}}\text{M27}$, $^{\text{B}}\text{Y24}$, and $^{\text{B}}\text{C23}$) that are well-resolved in the 1D spectrum. The conventional 1D pulse sequence (90°_x – SL_y – 180°_x) was used for that purpose. These amide and H^{α} $T_{1\rho}$ values were compared to the $T_{1\rho}$ values of the H^{α} protons of the corresponding residues measured by the 2D pulse sequence. The 1D values deviate from their 2D counterparts by an average of $\pm 8\%$, which is within the experimental error.

Comparison of $T_{1\rho}$ Values Obtained by 2D Using Two Different Spin-Lock Powers. The measured $T_{1\rho}$ values are

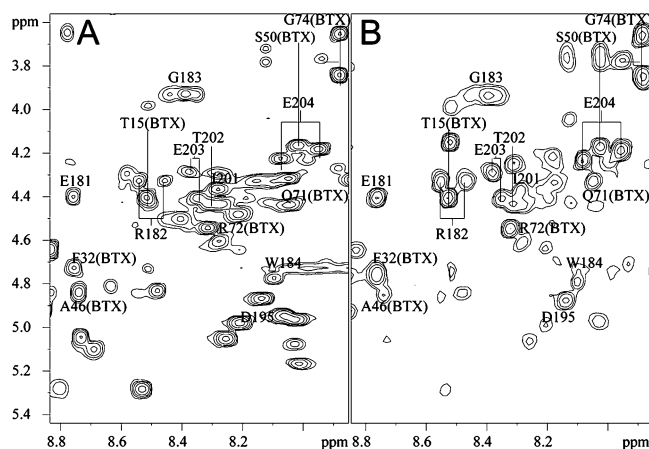


FIGURE 5: $T_{1\rho}$ -filtered HOHAHA spectra of the α -BTX-AChR peptide complex measured with different durations of the WALTZ pulse train. (A) A spectrum recorded with a WALTZ pulse train and trim pulses with a total duration of 30 ms. (B) A spectrum recorded with a WALTZ pulse train and trim pulses with a total duration of 200 ms. In both experiments, a spin lock with a duration of 25 ms was applied after the initial 90° pulse and prior to the evolution period. Notice the fewer H^α cross-peaks in spectrum B in comparison with spectrum A.

sensitive to exchange processes, for example, equilibrium between two conformations, occurring on the millisecond time scale (17, 51). To check the reproducibility of the $T_{1\rho}$ measurements and to rule out any significant exchange contribution to the measured relaxation rates, we repeated the $T_{1\rho}$ measurements using a 5 kHz spin-lock power. Most importantly, the overall $T_{1\rho}$ profile is very similar to that measured with a spin-lock of 8.3 kHz, suggesting that there is no significant contribution of exchange processes to the relaxation. The systematic increase of 10% in $T_{1\rho}$ values is expected due to the smaller tilt angle of the rotating frame when a weaker SL pulse is applied (52).

DISCUSSION

Comparison with Relaxation Studies of Other α -Neurotoxins. Three-finger toxins have been the focus of numerous studies. Interest in this family of toxins has been motivated mainly by their high-affinity binding to AChR. The dynamics of a few snake three-finger neurotoxins in their free form only were studied by NMR. The dynamics of the three-finger short snake neurotoxin toxin α (46) and the long neurotoxin LSIII (53) were studied in detail by NMR using natural abundance ^{13}C and by molecular dynamics. The dynamics of toxin α were studied also using ^{15}N -labeled protein (54). The largest mobility, as reflected by the NMR order parameters and by molecular dynamics simulations, was found for residues at the tip of the second finger. Using model-free analysis, this region was characterized by large-amplitude motions on the pico- and nanosecond time scale (53). The C-terminal segment was found to be rigid in the short neurotoxin toxin α and highly mobile in the long neurotoxin LSIII. The other regions that exhibited high flexibility were the tip of loop I and the N-terminal strand of loop III and the tip of this loop. This is in excellent agreement with the unusually long $T_{1\rho}$ relaxation times (≥ 100 ms) observed in this study for $^{\text{B}}\text{S35}$ and $^{\text{B}}\text{R36}$ at the tip of the second finger (Figure 6) and for $^{\text{B}}\text{Q71}$, $^{\text{B}}\text{R72}$, and $^{\text{B}}\text{G74}$ at the C-terminus. The higher than average $T_{1\rho}$ relaxation times (≥ 60 ms) observed for residues at the tip of the first

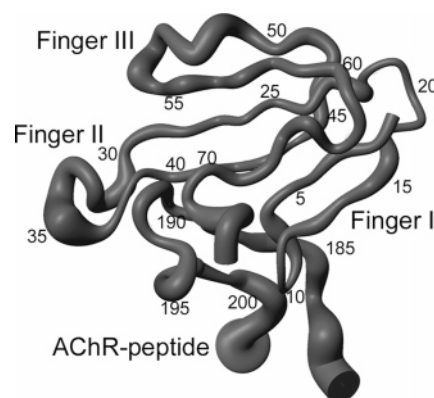


FIGURE 6: Variation in $T_{1\rho}$ values drawn on the backbone structure of the α -BTX-AChR peptide complex. The thickness of the C^α trace is proportional to the $T_{1\rho}$ values of the toxin and peptide residues.

finger and at the third finger are also in good agreement with the earlier dynamics studies.

Changes in Toxin Mobility upon Binding of the AChR Peptide. In the absence of a three-dimensional structure of the complexes of toxin α and LSIII with AChR or AChR peptides, mutational analysis was previously used to locate the segments of these toxins involved in binding. Correlation has been found between the toxins' segments implicated in binding and the flexibility observed by NMR. The NMR structure of the α -BTX complex with the AChR peptide, and the derived model for the α -BTX complex with the extracellular domain of the receptor, enable for the first time a comparison of the $T_{1\rho}$ relaxation times of the free toxin to those of the bound toxin and a derivation of correlations between changes in relaxation times and interactions with AChR.

When the AChR peptide binds, the average $T_{1\rho}$ of α -BTX in the β -strands decreases from 37 to 28 ms ($T_{1\rho}$ ratio of 1.32) mostly due to the increase in the molecular mass from ~ 8 to ~ 11.1 kDa. The $T_{1\rho}$ ratios are comparable to the reciprocal of the molecular weight ratio (1.39). As reflected by the $T_{1\rho}$ values in Figure 3, several larger than average changes in the toxin relaxation times occur upon binding of the α -AChR peptide. The major change occurs in residues $^{\text{B}}\text{T6}$, $^{\text{B}}\text{A7}$, and $^{\text{B}}\text{I11}$ of the first finger, in $^{\text{B}}\text{R36}$ and $^{\text{B}}\text{K38}$ of the second fingertip, and in $^{\text{B}}\text{K70}$ – $^{\text{B}}\text{G74}$ of the C-terminus. All residues exhibiting a considerably larger than average decrease in $T_{1\rho}$ coincide with the toxin regions shown to interact with the AChR peptide, namely, $^{\text{B}}\text{S5}$ – $^{\text{B}}\text{T12}$, $^{\text{B}}\text{R36}$ – $^{\text{B}}\text{L42}$, and $^{\text{B}}\text{H68}$ – $^{\text{B}}\text{Q71}$ (33). The observed changes in $T_{1\rho}$ probably reflect a significant change in mobility due to interactions with the AChR peptide. Residues located at the tip of toxin finger I play an important role in binding the AChR peptide. Once binding has occurred, the increases in the fraction of buried surface of residues $^{\text{B}}\text{T6}$, $^{\text{B}}\text{A7}$, and $^{\text{B}}\text{I11}$ are 23, 67, and 13%, respectively (33). These residues were also shown to form multiple interactions with peptides and mimotopes of the major interacting determinant of the α -subunit of AChR (33, 48, 55–58). $^{\text{B}}\text{R36}$ is one of the very few invariant residues in snake α -neurotoxins, and it was previously suggested to mimic acetylcholine in its interactions with AChR (33, 59, 60). The decrease in the $T_{1\rho}$ relaxation time of $^{\text{B}}\text{R36}$ can be explained by its extensive interactions with $^{\text{A}}\text{Y190}$ and $^{\text{A}}\text{Y198}$ of the AChR peptide

(33). B K38 was found to interact with A Y190 and A T191. Moreover, when the AChR peptide binds to α -BTX, the C-terminal β -strand of the α -BTX second finger are elongated and the B K38– B V40 segment which is part of the elongated β -strand forms an intermolecular β -sheet with the β -hairpin formed by the AChR peptide. The formation of the intermolecular β -sheet should contribute to the dramatic change in the relaxation properties of B K38. C-Terminal residues B H68– B Q71 interact strongly with the AChR peptide. Upon binding, residues B H68, B K70, and B Q71 experience an increase in the fraction of buried surface of 12, 36, and 41%, respectively (33), in accord with the decrease in $T_{1\rho}$. The C-terminal segment was also found to form many interactions in structural studies of α -BTX complexes with AChR peptides and mimotopes (33, 48, 55–58, 61), and truncation of C-terminal residues B H68– B G74 leads to a 7-fold decrease in the apparent binding affinity for the receptor (60).

Biological Role of Toxin Fingertip Dynamics. The NMR structure of α -BTX with the AChR peptide and the NMR-derived model for the AChR complex with α -BTX revealed for the first time that the invariant B R36 occupies the binding site for acetylcholine (33). This is contrary to suggestions that neurotoxins did not bind to the ACh binding site but rather sterically covered the entrance to the ligand binding pocket (53, 56). The ACh binding sites are located in two deep pockets at the α - γ and α - δ subunit interfaces. The flexibility of B R36 along with that of the invariant glycine B G37 on the second fingertip is probably required for the penetration of the arginine side chain into this deep pocket and for an optimal fit. The flexibility of the C-terminal segment which encircles the AChR β -hairpin formed by residues 184–200 may be required for optimal binding. Interestingly, five residues retained considerably long $T_{1\rho}$ relaxation times in the bound toxin, indicative of considerable mobility (Figures 3B and 6). These residues comprise B S34 and B S35 at the tip of second finger as well as B S50, B K51, and B Y54 at the N-terminal strand of the third finger. These residues were not found to interact with the AChR peptide and do not display exceptional changes in their relaxation times (Figure 3C). However, these five residues were predicted to interact with the γ - and δ -subunits in the NMR-derived model of the heteropentameric AChR complex with α -BTX (33). The flexibility of the residues involved in AChR binding could be important for the optimal fit with the AChR of different species and for the penetration of the second finger into the cleft between the $\alpha\gamma$ and $\alpha\delta$ subunits and the insertion of B R36 into the deep and partially concealed pocket that serves for acetylcholine binding.

Applications. Proton magnetic relaxation measurements do not enjoy widespread popularity, perhaps because current 1D methods suffer from poor resolution and are suitable for only short peptides. Herein, we present a simple 2D method for measuring $T_{1\rho}$ relaxation times of protons in unlabeled proteins. The proposed experiment will facilitate the determination of the proton relaxation rates in unlabeled proteins. Comparison of the results of the $T_{1\rho}$ measurements with model-free analysis and molecular dynamics studies of neurotoxins reveals a correlation between proton $T_{1\rho}$ relaxation times that are considerably longer than the average $T_{1\rho}$ of the other protein protons with large amplitude motion on the pico- to nanosecond time scale. Thus, proton $T_{1\rho}$ measurements can be used to obtain qualitative information about segments of

the proteins that are unstructured or have unusual flexibility. As such, $T_{1\rho}$ measurements can be used to define the boundaries of epitopes within longer peptides that interact strongly with antibodies, receptors or other proteins.

ACKNOWLEDGMENT

We thank Profs. Fred Naider and Eva Meirovitch, for helpful comments and assistance in the preparation of the manuscript.

REFERENCES

1. Torchia, D., Lyerla, J., and Quattrone, A. J. (1975) Molecular dynamics and structure of the random coil and helical states of the collagen peptide, α 1-CB2, as determined by ^{13}C magnetic resonance, *Biochemistry* 14, 887–900.
2. Jardetzky, O., and Roberts, G. C. K. (1981) *NMR in molecular biology*, Academic Press, New York.
3. Weiss, M. A., Eliason, J. L., and States, D. J. (1984) Dynamic filtering by two-dimensional ^1H NMR with application to phage λ repressor, *Proc. Natl. Acad. Sci. U.S.A.* 81, 6019–23.
4. Ishima, R., Wingfield, P. T., Stahl, S. J., Kaufman, J. D., and Torchia, D. A. (1998) Using amide ^1H and ^{15}N transverse relaxation to detect millisecond time-scale motions in perdeuterated proteins: Application to HIV-1 protease, *J. Am. Chem. Soc.* 120, 10534–42.
5. Boulat, B., and Bodenhausen, G. (1993) Measurement of proton relaxation rates in proteins, *J. Biomol. NMR* 3, 335–48.
6. Millet, O., Chiarparin, E., Pelulessy, P., Pons, M., and Bodenhausen, G. (1999) Measurement of relaxation rates of N^{H} and H^{α} backbone protons in proteins with tailored initial conditions, *J. Magn. Reson.* 139, 434–8.
7. Boulat, B., Konrat, R., Burghardt, I., and Bodenhausen, G. (1992) Measurement of relaxation rates in crowded NMR spectra by selective coherence transfer, *J. Magn. Reson.* 114, 5412–4.
8. Arseniev, A. S., Sobol, A. G., and Bystrov, V. F. (1986) T_1 relaxation measurement by two-dimensional NMR spectroscopy, *J. Mol. Graphics* 70, 427–35.
9. Kay, L. E., and Prestegard, J. H. (1988) Spin–lattice relaxation rates of coupled spins from 2D accordion spectroscopy, *J. Magn. Reson.* 77, 599–605.
10. Bodenhausen, G., and Ernst, R. R. (1981) The accordion experiment, a simple approach to three-dimensional NMR spectroscopy, *J. Magn. Reson.* 45, 367.
11. Bodenhausen, G., and Ernst, R. R. (1982) Direct determination of rate constants of slow dynamic processes by two-dimensional “accordion” spectroscopy in nuclear magnetic resonance, *J. Am. Chem. Soc.* 104, 1304.
12. Frederick, A. F., Kay, L. E., and Prestegard, J. H. (1988) Location of divalent ion sites in acyl carrier protein using relaxation perturbed 2D NMR, *FEBS Lett.* 238, 43–8.
13. Ulmer, T. S., Campbell, I. D., and Boyd, J. (2004) Amide proton relaxation measurements employing a highly deuterated protein, *J. Magn. Reson.* 166, 190–201.
14. Wang, Y. S., and Ikuta, S. (1989) Proton on-resonance rotating frame spin–lattice relaxation measurements of B and Z double-helical oligodeoxyribonucleotides in solution, *J. Am. Chem. Soc.* 111, 1243–8.
15. Schmitz, U., Sethson, I., Egan, W. M., and James, T. L. (1992) Solution structure of a DNA octamer containing the Pribnow box via restrained molecular dynamics simulation with distance and torsion angle constraints derived from two-dimensional nuclear magnetic resonance spectral fitting, *J. Mol. Biol.* 227, 510–31.
16. Kennedy, M. A., Nuutero, S. T., Davis, J. T., Drobny, G. P., and Reid, B. R. (1993) Mobility at the Tpa cleavage site in the T3A3-containing AhaIII and PmeI restriction sequences, *Biochemistry* 32, 8022–35.
17. Bleich, H. E., and Glasel, J. A. (1978) Rotating frame spin–lattice relaxation experiments and the problem of intramolecular motions of peptides in solution, *Biopolymers* 17, 2445–57.
18. Bleich, H. E., Day, A. R., Freer, R. J., and Glasel, J. A. (1979) NMR rotating frame relaxation studies of intramolecular motion in peptides. Tyrosine ring motion in methionine-enkephalin, *Biochem. Biophys. Res. Commun.* 87, 1146–53.
19. Kopple, K., Bhandary, K. K., Kartha, G., Wang, Y. S., and Parameswaran, K. N. (1986) Conformations of cyclic octapeptides. 3. Cyclo-(D-Ala-Gly-Pro-Phe) $_2$. Conformations in crystals and a

- $T_{1\rho}$ examination of internal mobility in solution, *J. Am. Chem. Soc.* **108**, 4637–42.
20. Kopple, K., Wang, S. Y., Cheng, A. G., and Bhandary, K. K. (1988) Conformations of cyclic octapeptides. 5. Crystal structure of cyclo(Cys-Gly-Pro-Phe)₂ and rotating frame relaxation ($T_{1\rho}$) NMR studies of internal mobility in cyclic octapeptides, *J. Am. Chem. Soc.* **110**, 4168–76.
 21. Scheucher, J., and Wijmenga, S. S. (2002) How to detect internal motion by homonuclear NMR, *J. Am. Chem. Soc.* **124**, 5881–9.
 22. Karlin, A. (1993) Structure of nicotinic acetylcholine receptors, *Curr. Opin. Neurobiol.* **3**, 299–309.
 23. Corringer, P. J., Le Novère, N., and Changeux, J. P. (2000) Nicotinic receptors at the amino acid level, *Annu. Rev. Pharmacol. Toxicol.* **40**, 431–58.
 24. Blount, P., and Merlie, J. P. (1989) Molecular basis of the two nonequivalent ligand binding sites of the muscle nicotinic acetylcholine receptor, *Neuron* **3**, 349–57.
 25. Haggerty, J. G., and Froehner, S. C. (1981) Restoration of ¹²⁵I- α -bungarotoxin binding activity to the α subunit of *Torpedo* acetylcholine receptor isolated by gel electrophoresis in sodium dodecyl sulfate, *J. Biol. Chem.* **256**, 8294–7.
 26. Wilson, P. T., Hawrot, E., and Lentz, T. L. (1988) Distribution of α -bungarotoxin binding sites over residues 173–204 of the α subunit of the acetylcholine receptor, *Mol. Pharmacol.* **34**, 643–50.
 27. Wilson, P. T., Lentz, T. L., and Hawrot, E. (1985) Determination of the primary amino acid sequence specifying the α -bungarotoxin binding site on the α subunit of the acetylcholine receptor from *Torpedo californica*, *Proc. Natl. Acad. Sci. U.S.A.* **82**, 8790–4.
 28. Wilson, P. T., and Lentz, T. L. (1988) Binding of α -bungarotoxin to synthetic peptides corresponding to residues 173–204 of the α subunit of *Torpedo*, calf, and human acetylcholine receptor and restoration of high-affinity binding by sodium dodecyl sulfate, *Biochemistry* **27**, 6667–74.
 29. Ralston, S., Sarin, V., Thanh, H. L., Rivier, J., Fox, J. L., and Lindstrom, J. (1987) Synthetic peptides used to locate the α -bungarotoxin binding site and immunogenic regions on α subunits of the nicotinic acetylcholine receptor, *Biochemistry* **26**, 3261–6.
 30. Conti-Tronconi, B. M., Tang, F., Diethelm, B. M., Spencer, S. R., Reinhardt-Maelicke, S., and Maelicke, A. (1990) Mapping of a cholinergic binding site by means of synthetic peptides, monoclonal antibodies, and α -bungarotoxin, *Biochemistry* **29**, 6221–30.
 31. Neumann, D., Barchan, D., Safran, A., Gershoni, J. M., and Fuchs, S. (1986) Mapping of the α -bungarotoxin binding site within the α subunit of the acetylcholine receptor, *Proc. Natl. Acad. Sci. U.S.A.* **83**, 3008–11.
 32. Samson, A. O., Chill, J. H., Rodriguez, E., Scherf, T., and Anglister, J. (2001) NMR mapping and secondary structure determination of the major acetylcholine receptor α -subunit determinant interacting with α -bungarotoxin, *Biochemistry* **40**, 5464–73.
 33. Samson, A., Scherf, T., Eisenstein, M., Chill, J., and Anglister, J. (2002) The mechanism for acetylcholine receptor inhibition by α -neurotoxins and species-specific resistance to α -bungarotoxin revealed by NMR, *Neuron* **35**, 319–32.
 34. Aronheim, A., Eshel, Y., Mosckovitz, R., and Gershoni, J. M. (1988) Characterization of the binding of α -bungarotoxin to bacterially expressed cholinergic binding sites, *J. Biol. Chem.* **263**, 9933–7.
 35. Scherf, T., and Anglister, J. (1993) A $T_{1\rho}$ -filtered two-dimensional transferred NOE spectrum for studying antibody interactions with peptide antigens, *Biophys. J.* **64**, 754–61.
 36. Zvi, A., Kustanovich, I., Feigelson, D., Levy, R., Eisenstein, M., Matsushita, S., Richalet-Secordel, P., Regenmortel, M. H., and Anglister, J. (1995) NMR mapping of the antigenic determinant recognized by an anti-gp120, human immunodeficiency virus neutralizing antibody, *Eur. J. Biochem.* **229**, 178–87.
 37. Braunschweiler, L., and Ernst, R. R. (1983) Coherence transfer by isotropic mixing: Application to proton correlation spectroscopy, *J. Magn. Reson.* **53**, 521–8.
 38. Bax, A., and Davis, D. G. (1985) MLEV-17-based two-dimensional homonuclear magnetization transfer spectroscopy, *J. Magn. Reson.* **65**, 335.
 39. Shaka, A. J., Keeler, J., and Freeman, R. (1983) Evaluation of a new broadband decoupling sequence: WALTZ-16, *J. Magn. Reson.* **53**, 313–40.
 40. Piotto, M., Saudek, V., and Sklenar, V. (1992) Gradient-tailored excitation for single-quantum NMR spectroscopy of aqueous solutions, *J. Biomol. NMR* **2**, 661–5.
 41. Delaglio, F., Grzesiek, S., Vuister, G. W., Zhu, G., Pfeifer, J., and Bax, A. (1995) NMRPipe: A multidimensional spectral processing system based on UNIX pipes, *J. Biomol. NMR* **6**, 277–93.
 42. Wüthrich, K. (1986) *NMR of Proteins and Nucleic Acids*, Wiley, New York.
 43. Koradi, R., Billeter, M., and Wüthrich, K. (1996) MOLMOL: A program for display and analysis of macromolecular structures, *J. Mol. Graphics* **14**, 51–5, 29–32.
 44. Werbelow, L. G., and Grant, D. M. (1977) Intramolecular dipolar relaxation in multispin systems, *Adv. Magn. Reson.* **9**, 189–299.
 45. Vold, R. L., and Vold, R. R. (1978) Nuclear magnetic relaxation in coupled spin systems, *Prog. NMR Spectrosc.* **12**, 79–113.
 46. Guenneugues, M., Gilquin, B., Wolff, N., Menez, A., and Zinn-Justin, S. (1999) Internal motion time scales of a small, highly stable and disulfide-rich protein: A ¹⁵N, ¹³C NMR and molecular dynamics study, *J. Biomol. NMR* **14**, 47–66.
 47. Gilquin, B., Bourgoin, M., Menez, R., Le Du, M. H., Servent, D., Zinn-Justin, S., and Menez, A. (2003) Motions and structural variability within toxins: Implication for their use as scaffolds for protein engineering, *Protein Sci.* **12**, 266–77.
 48. Basus, V. J., Song, G., and Hawrot, E. (1993) NMR solution structure of an α -bungarotoxin/nicotinic receptor peptide complex, *Biochemistry* **32**, 12290–8.
 49. Finerty, P. J., Jr., Mittermaier, A. K., Muhandiram, R., Kay, L. E., and Forman-Kay, J. D. (2005) NMR dynamics-derived insights into the binding properties of a peptide interacting with an SH2 domain, *Biochemistry* **44**, 694–703.
 50. Valeur, B., Jarry, J., Geny, F., and Monnerie, L. (1975) Dynamics of macromolecular chains. II. Orientation relaxation generated by elementary three-bond motions and notion of an independent kinetic segment, *J. Polym. Sci., Part B: Polym. Phys.* **13**, 675–82.
 51. Deverell, C., Morgan, R. E., and Strange, J. H. (1970) Studies of chemical exchange by nuclear magnetic relaxation in the rotating frame, *Mol. Phys.* **18**, 553–9.
 52. Cavanagh, J., Fairbrother, W. J., Palmer, A. G., and Skelton, N. J. (1996) *Protein NMR Spectroscopy: Principles and Practice*, Academic Press, San Diego.
 53. Connolly, P. J., Stern, A. S., Turner, C. J., and Hoch, J. C. (2003) Molecular dynamics of the long neurotoxin LSIII, *Biochemistry* **42**, 14443–51.
 54. Guenneugues, M., Drevet, P., Pinkasfeld, S., Gilquin, B., Menez, A., and Zinn-Justin, S. (1997) Picosecond to hour time scale dynamics of a “three finger” toxin: Correlation with its toxic and antigenic properties, *Biochemistry* **36**, 16097–108.
 55. Scarselli, M., Spiga, O., Ciutti, A., Bernini, A., Bracci, L., Lelli, B., Lozzi, L., Calamandrei, D., Di Maro, D., Klein, S., and Niccolai, N. (2002) NMR structure of α -bungarotoxin free and bound to a mimotope of the nicotinic acetylcholine receptor, *Biochemistry* **41**, 1457–63.
 56. Harel, M., Kasher, R., Nicolas, A., Guss, J. M., Balass, M., Fridkin, M., Smit, A. B., Brejc, K., Sixma, T. K., Katchalski-Katzir, E., Sussman, J. L., and Fuchs, S. (2001) The binding site of acetylcholine receptor as visualized in the X-ray structure of a complex between α -bungarotoxin and a mimotope peptide, *Neuron* **32**, 265–75.
 57. Scherf, T., Balass, M., Fuchs, S., Katchalski-Katzir, E., and Anglister, J. (1997) Three-dimensional solution structure of the complex of α -bungarotoxin with a library-derived peptide, *Proc. Natl. Acad. Sci. U.S.A.* **94**, 6059–64.
 58. Scherf, T., Kasher, R., Balass, M., Fridkin, M., Fuchs, S., and Katchalski-Katzir, E. (2001) A β -hairpin structure in a 13-mer peptide that binds α -bungarotoxin with high affinity and neutralizes its toxicity, *Proc. Natl. Acad. Sci. U.S.A.* **98**, 6629–34.
 59. Karlsson, E. (1979) in *Handbook of experimental pharmacology* (Lee, C. Y., Ed.) pp 159–212, Springer-Verlag, Berlin.
 60. Rosenthal, J. A., Levandoski, M. M., Chang, B., Potts, J. F., Shi, Q. L., and Hawrot, E. (1999) The functional role of positively charged amino acid side chains in α -bungarotoxin revealed by site-directed mutagenesis of a His-tagged recombinant α -bungarotoxin, *Biochemistry* **38**, 7847–55.
 61. Zeng, H., Moise, L., Grant, M. A., and Hawrot, E. (2001) The solution structure of the complex formed between α -bungarotoxin and an 18mer cognate peptide derived from the α 1 subunit of the nicotinic acetylcholine receptor from *Torpedo californica*, *J. Biol. Chem.* **18**, 18.